

THE ANATOMY OF AN EXTREME STARBURST WITHIN 1.3 Gyr OF THE BIG BANG REVEALED BY ALMA*

C. L. CARILLI^{1,2}, D. RIECHERS³, F. WALTER⁴, R. MAIOLINO², J. WAGG⁵, L. LENTATI², R. MCMAHON⁶, AND A. WOLFE⁷

¹ National Radio Astronomy Observatory, P.O. Box 0, Socorro, NM 87801, USA; ccarilli@aoc.nrao.edu

² Astrophysics Group, Cavendish Laboratory, J. J. Thomson Avenue, Cambridge CB3 0HE, UK

³ Astronomy Department, California Institute of Technology, MC 249-17, 1200 East California Boulevard, Pasadena, CA 91125, USA

⁴ Max-Planck-Institut für Astronomie, Königstuhl 17, D-69117 Heidelberg, Germany

⁵ European Southern Observatory, Alonso de Cordova 3107, Vitacura, Casilla 19001, Santiago 19, Chile

⁶ Institute of Astronomy, University of Cambridge, Madingley Road, Cambridge CB3 0HA, UK

⁷ Department of Physics and Center for Astrophysics and Space Sciences, University of California, San Diego, La Jolla, CA 92093, USA

Received 2012 July 9; accepted 2012 December 4; published 2013 January 16

ABSTRACT

We present further analysis of the [C II] 158 μm fine structure line and thermal dust continuum emission from the archetype extreme starburst/active galactic nucleus (AGN) group of galaxies in the early universe, BRI 1202–0725 at $z = 4.7$, using the Atacama Large Millimeter Array. The group has long been noted for having a closely separated (26 kpc in projection) FIR–hyperluminous quasar host galaxy and an optically obscured submillimeter galaxy (SMG). A short ALMA test observation reveals a rich laboratory for the study of the myriad processes involved in clustered massive galaxy formation in the early universe. Strong [C II] emission from the SMG and the quasar have been reported earlier by Wagg et al. based on these observations. In this paper, we examine in more detail the imaging results from the ALMA observations, including velocity channel images, position–velocity plots, and line moment images. We present detections of [C II] emission from two Ly α -selected galaxies in the group, demonstrating the relative ease with which ALMA can detect the [C II] emission from lower star formation rate galaxies at high redshift. Imaging of the [C II] emission shows a clear velocity gradient across the SMG, possibly indicating rotation or a more complex dynamical system on a scale ~ 10 kpc. There is evidence in the quasar spectrum and images for a possible outflow toward the southwest, as well as more extended emission (a “bridge”), between the quasar and the SMG, although the latter could simply be emission from Ly α -1 blending with that of the quasar at the limited spatial resolution of the current observations. These results provide an unprecedented view of a major merger of gas-rich galaxies driving extreme starbursts and AGN accretion during the formation of massive galaxies and supermassive black holes within 1.3 Gyr of the big bang.

Key words: galaxies: formation – galaxies: high-redshift – galaxies: starburst – radio lines: galaxies – submillimeter: galaxies

1. INTRODUCTION

The last decade has seen the solidification of two important conclusions concerning massive galaxy formation. The first is that massive galaxies form most of their stars at early times, and the more massive, the earlier. This point has been accentuated by the observation of old spheroidal galaxies at $z \sim 2$ –3, thereby requiring active star formation at even higher redshifts (Kurk 2009; Andreon & Huertas-Company 2011). Second, the observed correlation between central black hole and spheroidal galaxy mass suggests a causal connection between the formation of supermassive black holes (SMBH) and their host galaxies (Haaring & Rix 2004).

Large-scale cosmological simulations show that massive galaxies and SMBH can form at high- z via gas-rich mergers, driving extreme starbursts, and rapid accretion onto the black holes and subsequent black hole mergers (Li et al. 2007). These processes occur in the densest, i.e., most biased, regions in the early universe. The systems evolve into large galaxies in rich clusters at low- z . More recent simulations suggest that cold accretion from the IGM may also play a role in, and possibly even dominate, the gas resupply (Khandai et al. 2012). As the SMBH builds, feedback from the active galactic nucleus

(AGN) expels gas from the galaxy, and hinders further accretion, thereby terminating star formation in the galaxy.

Galaxies detected in submillimeter surveys with mJy sensitivity are important in this regard, representing massive starburst galaxies in the distant universe. These include the submillimeter galaxies (SMGs) and about 1/3 of quasar host galaxies at $z > 2$ (Wang et al. 2011, 2010a, 2010b; Blain et al. 2002). These systems are hyper-luminous infrared galaxies ($L_{\text{FIR}} \sim 10^{13} L_{\odot}$). The implied star formation rates are $> 10^3 M_{\odot} \text{ year}^{-1}$ based on the FIR emission. At this rate, a substantial fraction of the stars in the galaxy can form on timescales $\leq 10^8$ years.

The compact group of galaxies BRI 1202–0725 was one of the first $z > 4$ submillimeter-bright systems discovered (Isaak et al. 1994) and remains the archetype for major starbursts in gas-rich mergers in the early universe. The system includes an optically selected, broad absorption line quasar with $M_{\text{BH}} \sim 10^9 M_{\odot}$ at a redshift of $z = 4.695$, and an optically undetected SMG located 4'' (26 kpc) northwest of the quasar at $z = 4.692$ (Omont et al. 1996; Hu et al. 1996). Both sources are hyper-luminous FIR galaxies (Omont et al. 1996; Iono et al. 2006; Yun et al. 2000). Both sources have been detected in CO line emission, with implied gas masses $M(\text{H}_2) \sim 5 \times 10^{10} (\alpha/0.8) M_{\odot}$ (Salome et al. 2012; Carilli et al. 2002; Ohta et al. 1996; Omont et al. 1996), assuming a CO luminosity to gas mass conversion factor, $\alpha = 0.8 M_{\odot} (\text{K km s}^{-1} \text{ pc}^2)^{-1}$, appropriate for star-forming galaxies (Solomon & Downes 1998). Both sources are detected in radio continuum emission, consistent with either a weak AGN or extreme star formation (Yun & Carilli 2002).

* ALMA is a partnership of ESO (representing its member states), NSF (USA) and NINS (Japan), together with NRC (Canada) and NSC and ASIAA (Taiwan), in cooperation with the Republic of Chile. The National Radio Astronomy Observatory is a facility of the National Science Foundation operated under cooperative agreement by Associated Universities, Inc.

Very high resolution CO and radio continuum imaging shows resolved emitting regions on scales $\sim 0''.3$, likely corresponding to compact starbursts in both galaxies on scales ~ 2 kpc (Carilli et al. 2002; Momjian et al. 2005; Yun & Carilli 2002).

The best CO observations of the BRI 1202–0725 system to date are by Salome et al. (2012). They find that the SMG appears extended, with two components separated by $\sim 0''.5$ east–west. The CO emission from the quasar also appears extended to the south by about $2''$. The CO excitation in both galaxies is high, suggesting warm (40–50 K), dense ($> 10^3$ cm $^{-3}$) gas.

Extended Ly α emission has been seen around the quasar, with a tail of emission extending from the quasar toward the SMG, terminating in an Ly α emitting galaxy about $2''.3$ northwest of the quasar (Hu et al. 1996; Ohta et al. 2000; Ohyama et al. 2004). This galaxy is designated Ly α -1 by Salome et al. (2012). Spectra of this galaxy yield a redshift of 4.702 ± 0.009 (Petitjean et al. 1996). The large uncertainty in the redshift reflects the fact that the Ly α profile for this galaxy is broad and complex. Continuum emission from Ly α -1 is detected in the *Hubble Space Telescope* (*HST*) *i*-band image (Hu et al. 1996). Klamer et al. (2004) discuss the possibility of jet-induced star formation in this system, although an extended radio jet has not been detected to date. A second galaxy has been detected in Ly α emission, and in the *HST i*-band image, located $2''.7$ southwest of the quasar (Hu et al. 1996, 1997; Fontana et al. 1996). Salome et al. (2012) designate this galaxy Ly α -2. Both of these galaxies appear extended on a scale $\sim 0''.5$ in the *HST* images, toward the quasar.

In an earlier paper, Wagg et al. (2012) presented an initial analysis of the [C II] and dust continuum emission from the SMG and the quasar host galaxy in BRI 1202–0725 using a test observation from ALMA. The [C II] 158 μ m line is typically the strongest emission line from cool gas in star-forming galaxies, and is a principle ISM gas coolant, tracing photon-dominated regions enveloping active star forming clouds, low-density ionized gas, and the cold neutral medium (Genzel & Cesarsky 2000; Stacey et al. 2010; Malhotra et al. 1997; Crawford et al. 1986). As such, the [C II] line is a key diagnostic of ISM energetics in early galaxies as well as of galaxy dynamics (Carilli & Walter 2013). Wagg et al. (2012) find that the [C II]/FIR luminosity ratio is relatively low in both the SMG and quasar, 8×10^{-4} and 2×10^{-4} , respectively. For comparison, the Milky Way has a value of 3×10^{-3} (Wright et al. 1991; Bennett et al. 1994). Low [C II]/FIR ratios are typically seen in extreme starburst environments, and may arise due to the high-radiation environment leading to substantially charged dust grains, and hence less efficient gas heating via photoelectric emission from the dust grains (Malhotra et al. 1997). Alternatively, Sargsyan et al. (2012) propose that a substantial contribution to dust heating by an AGN may lead to low ratios in very luminous systems, while Papadopoulos et al. (2010) suggest that optical depth effects at 158 μ m may also play a role.

In this paper, we present a more detailed analysis of the ALMA data, with a closer look at the imaging results based on self-calibration of the visibility data. We present spectra, channel images, moment images, and a position–velocity analysis. The [C II] imaging reveals a rich physical environment. Both Ly α emitting galaxies are also detected in [C II] emission. The SMG shows a clear velocity gradient in the atomic gas on a scale ~ 10 kpc, and the quasar shows evidence for atomic gas outflow, or a possible tidal feature to the southwest toward Ly α -2. There may even be a bridge of cool gas connecting the quasar and the SMG, although the presence of Ly α -1 confuses this possibility.

2. OBSERVATIONS

Observations were made of BRI 1202–0725 with the Atacama Large Millimeter Array during science testing and verification in 2012 January (see Wagg et al. 2012 for more details). These short observations (25 minutes on-source), with only 17 antennas, are already an order of magnitude more sensitive than any previous submillimeter line or continuum observations of the system. Observations were made with four dual-polarization bands of 2 GHz bandwidth each. The first band covered the [C II] line from the SMG and the quasar, with a central (sky) frequency of 333.960 GHz, corresponding to a redshift of $z = 4.6909$ for the [C II] 158 μ m line (rest frequency = 1900.539 GHz). The other bands were centered off the line by ~ 10 GHz, and these were used for continuum imaging. Hanning smoothing was applied on output from the correlator to the 128 channel per 2 GHz band spectral data.

Calibration of the data was performed using the Astronomical Image Processing System (AIPS). The source 3C279 was used as a flux density and phase calibrator, using the flux density at 340 GHz of 17 Jy derived by Wagg et al. (2012). 3C279 is located 13° from the target source. A 10 minute calibration cycle was employed during the observations, and the weather conditions were excellent, with gains stable to a few degrees and a few percent over the hour. The source 3C279 was also used for bandpass calibration, and the bandpass was smooth and stable, again to within a few percent and a few degrees except for a few edge channels in each band that were flagged.

The sensitivity of even the reduced array of ALMA is such that self-calibration could be employed using the continuum and line emission from BRI 1202–0725 (total continuum flux density of 37 mJy at 340 GHz). Amplitude and phase self-calibration was performed using a three minute averaging time for complex gain solutions.

Imaging was performed using a robust imaging scheme with $R = 1$ (Cornwell et al. 1999), for which the restoring Gaussian beam was $1''.2 \times 0''.8$ resolution (major axis north–south). For the spectral line data, the continuum was subtracted from the UV data using a CLEAN component model derived from the three off-line bands, before imaging and deconvolution.

3. RESULTS

Figure 1(a) shows the 340 GHz continuum emission from BRI 1202–0725, overlaid on the *HST i*-band image. For relative astrometry (optical–radio), we follow Carilli et al. (2002) by aligning the quasar position in the *HST*, Ly α , submillimeter continuum, and radio continuum images. Given the scatter in these positions, a rough estimate of the relative astrometry is $\sim 0''.25$.

The continuum emission from the SMG and quasar is unresolved (deconvolved sizes $< 0''.3$ derived from Gaussian fitting), with flux densities of 17 ± 2.5 mJy and 18 ± 2.7 mJy, respectively, including the 15% uncertainty in absolute gain calibration estimated by Wagg et al. (2012). The galaxy Ly α -2 to the southwest of the quasar is also detected in the continuum and is unresolved with a flux density 1.4 ± 0.2 mJy (see also Wagg et al. 2012). This submillimeter continuum source peaks $0''.4$ from Ly α -2, as seen on the *HST* image (Hu et al. 1996), although this galaxy appears extended in the *HST* image in the direction of the submillimeter source and the quasar by at least $0''.5$ (Figure 1(a)).

Figure 2 shows the channel images of the [C II] line, smoothed to a spectral resolution of 62.5 MHz ($= 56$ km s $^{-1}$). Spectra of the

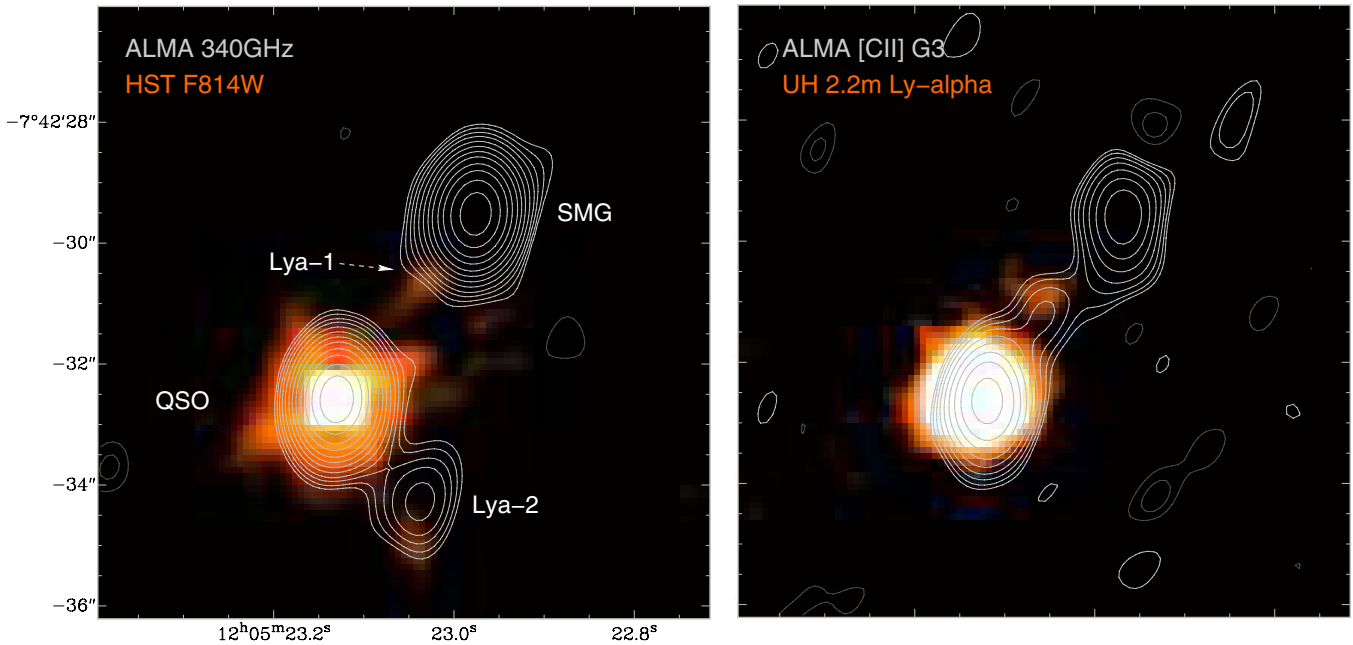


Figure 1. Left: white contours show the submillimeter continuum emission from BRI 1202-0725 at 340 GHz at $1''.2 \times 0''.8$ resolution (major axis north–south). Contour levels are a geometric progression in square root two, starting at $0.25 \text{ mJy beam}^{-1}$. Negative contours are dashed. The rms noise on the image is $0.1 \text{ mJy beam}^{-1}$. The color shows the *HST* F814W image of Hu et al. (1996). The SMG, quasar, Ly α -1, and Ly α -2 are indicated. Right: the integrated [C II] emission in the velocity range 0 km s^{-1} to 130 km s^{-1} (see Figures 2 and 3(c)). Contour levels are a geometric progression in square root two, starting at $1.0 \text{ mJy beam}^{-1}$. The color is the Ly α narrowband image from Hu et al. (1996). The Ly α image within $\sim 1''$ of the quasar is saturated. Note that saturation and diffraction spikes affect the *HST* and Ly α images within about a $1''$ radius of the quasar.

Table 1
BRI 1202-0725 Parameters

Source	Position ^a J2000	$S_{340 \text{ GHz}}$ (mJy)	[C II] Redshift ^b	Line Peak (mJy)	FWHM ^c (km s^{-1})
Quasar ^d	J120523.13–074232.6	18 ± 2.7	4.6942	24 ± 3.6	275
SMG	J120522.98–074229.5	17 ± 2.5	4.6915	16 ± 2.4	712
Ly α -1	J120523.06–074231.2	<0.3	4.6950	5.1 ± 0.7	56
Ly α -2 ^e	J120523.04–074234.3	1.4 ± 0.2	4.7055	3.7 ± 0.6	338

Notes.

^a Submillimeter continuum position, except for Ly α -1, which uses the [C II] line peak position.

^b Formal errors from Gaussian fitting on the redshifts are <0.0003 in all cases.

^c Formal errors from Gaussian fitting on the line widths are $\leq 15 \text{ km s}^{-1}$.

^d Redshift for single Gaussian fit (see Section 3.1).

^e This line is truncated in velocity, and hence the fit is highly uncertain, and the redshift is strictly a lower limit.

sources are shown in Figure 3 at 31.25 MHz spectral resolution ($=28 \text{ km s}^{-1}$).

Strong [C II] emission is seen from the SMG over essentially the full frequency range in the first band. Likewise, strong emission is seen from the quasar over a narrower frequency range. For reference, we have fit Gaussian models to the spectra, although admittedly the SMG spectrum is decidedly non-Gaussian. Results from the fitting are given in Table 1 (see Wagg et al. 2012 for more details on the SMG and quasar spectra).

Inspection of the [C II] channel images shows emission from the vicinity of Ly α -1, between the quasar and the SMG, in a few channels just above 0 km s^{-1} . Figure 1(b) shows the integrated emission in the velocity range 0 km s^{-1} to 100 km s^{-1} , with the Ly α image of Hu et al. (1996) in color. This apparent [C II] emission is seen along the direction of the extended Ly α tail from the quasar toward the SMG (Hu et al. 1997), peaking

close (within $0''.3$) to galaxy Ly α -1. A spectrum at this peak position near Ly α -1 is shown in Figure 3(c). The [C II] emission from Ly α -1 is narrow, with an FWHM $\sim 56 \text{ km s}^{-1}$, centered at $z = 4.6950$. Note that it is difficult to conclude based on these relatively low spatial resolution data whether this emission is truly extended between the quasar and Ly α -1, or simply blended by the limited spatial resolution. The [C II] emission around the quasar also appears extended in the direction of Ly α -2 in the channels around $+250 \text{ km s}^{-1}$ to $+300 \text{ km s}^{-1}$.

The two highest velocity channels in Figure 2 show [C II] emission from galaxy Ly α -2. Figure 3(d) shows the spectrum of this galaxy. Since the redshift of this galaxy was essentially unknown prior to the observations, the spectral coverage truncates some unknown fraction of the line at high velocity (low frequency). Hence, we do not know the full velocity extent nor total luminosity of the [C II] emission for Ly α -2, and the redshift is strictly a lower limit.

Figure 4 shows the iso-velocity image (moment 1 = intensity-weighted mean velocity) of the [C II] emission made using a 3.5σ blanking level. There is a clear east–west velocity gradient across the SMG. This can be seen in the channel images (Figure 2), where the peak of the line emission moves by about $1''.7$ east to west from low to high velocities. The tail of emission to the north of the quasar toward Ly α -1 is also seen, as well as the extended emission to the southwest of the quasar toward Ly α 2.

Figure 5 shows a position–velocity (PV) plot along the major axis (east–west) of the SMG. The E–W velocity gradient is clear, as well as a twist in the line of nodes at the extrema in velocity. Such a twist could signal a warped disk in atomic gas.

4. ANALYSIS

Wagg et al. (2012) present a detailed analysis of the main [C II] line and dust continuum emission from the quasar and SMG in

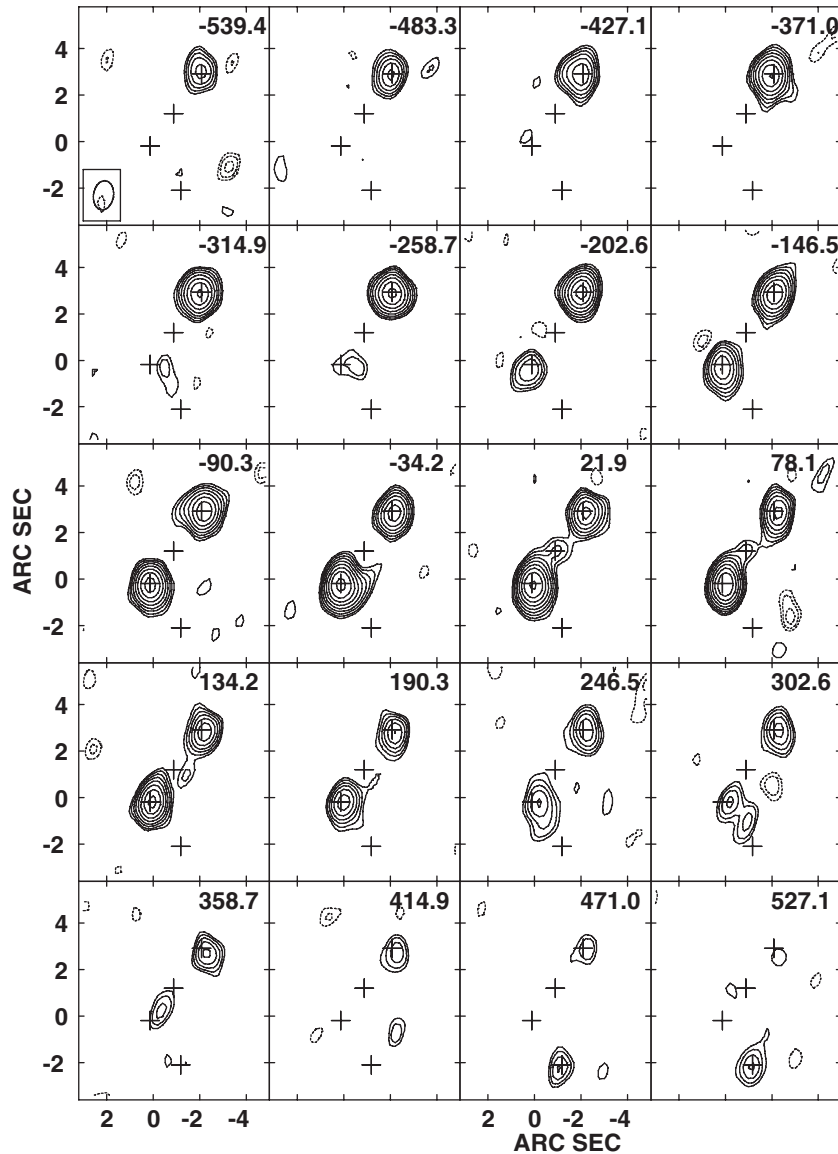


Figure 2. [C II] channel images at 62.5 MHz ($=56 \text{ km s}^{-1}$) per channel, and $1''.2 \times 0''.8$ resolution (major axis north–south). The channels are labeled in velocity (km s^{-1}), where zero velocity corresponds to $z = 4.6941$. Contour levels are a geometric progression in square root two, starting at $1.5 \text{ mJy beam}^{-1}$. Negative contours are dashed. The crosses show the positions of the peak in the submillimeter continuum emission from the SMG, quasar, and $\text{Ly}\alpha$ -2, and the [C II] peak in $\text{Ly}\alpha$ -1. The continuum derived from the off-line bands has been subtracted. The rms noise is $0.64 \text{ mJy beam}^{-1} \text{ channel}^{-1}$.

BRI 1202–0725. Herein, we focus on the [C II] imaging, and in particular, the extended emission from the SMG, quasar, and the $\text{Ly}\alpha$ emitting galaxies.

4.1. SMG Dynamics

The isovelocity contours of the [C II] emission from the SMG show a gradient of 525 km s^{-1} over $\sim 1''.7$ (Figure 4). If due to simple rotation, then this would imply a dynamical mass of $3.6 \times 10^{11} [\sin(i)/\sin(45)]^{-2} M_{\odot}$ to a radius of 5.5 kpc. This mass is an order of magnitude higher than the molecular gas mass (Carilli et al. 2002), unless one adopts the five times larger CO luminosity to gas mass conversion factor for the Milky Way relative to the nuclear starburst value. However, recent observations suggest that a starburst conversion factor is clearly favored in SMGs (see Carilli & Walter 2013 for a review).

Perhaps the simplest conclusion is that the velocity gradient in the SMG is not due to rotation. Salome et al. (2012) find that the CO 5–4 line profile for the SMG appears more like

a double-line system as opposed to the more gradual gradient seen at higher velocities in the [C II] line spectrum. Likewise, the east–west PV for the SMG in CO 5–4 shows a more broken distribution, with a dip, then plateau to high velocity. The [C II] shows a more continuous distribution. Salome et al. conclude that the SMG itself may in fact be an end-stage merger of two gas rich galaxies.

4.2. Quasar Outflow

The quasar [C II] emission line is well fit by a Gaussian, except at the high-velocity end of the spectrum, where there appears to be a broad wing. Figure 3 shows a double Gaussian fit to the spectrum including this broad wing. In this case, the main component has a redshift of 4.6941, a peak of 24 mJy, and an $\text{FWHM} = 274 \text{ km s}^{-1}$. The second component for the wing has a peak flux density of 2.4 mJy, centered at $z = 4.6967$, or 141 km s^{-1} from the quasar redshift, and an $\text{FWHM} = 395 \text{ km s}^{-1}$ (Figure 2(b)). Inspection of the channel images

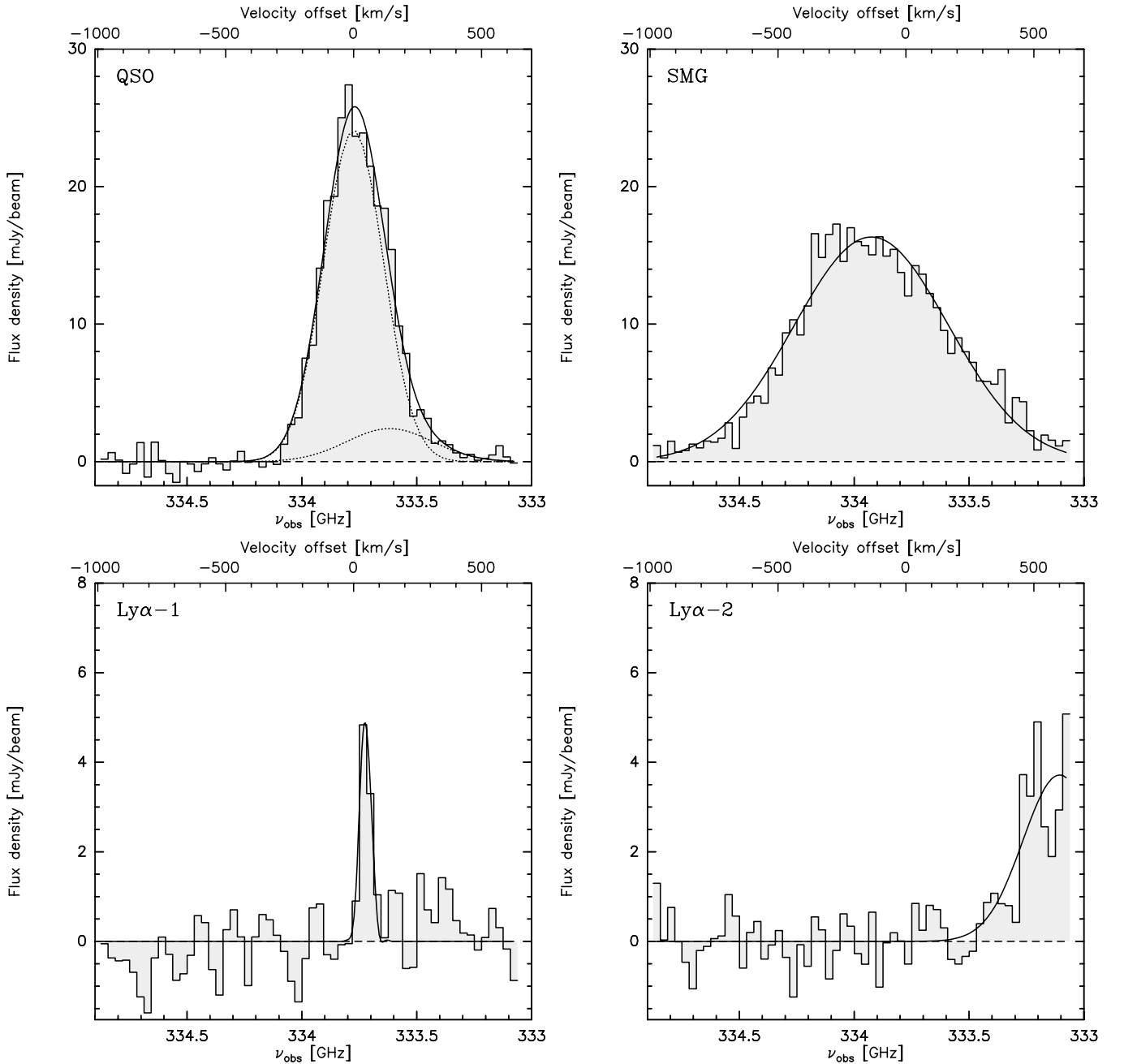


Figure 3. Spectra of the four galaxies in the BRI 1202–0725 system at 31.25 MHz spectral resolution ($=28 \text{ km s}^{-1}$). (a)–(d) The SMG, quasar, Ly α -1, and Ly α -2, respectively. The continuum derived from the offline IFs has been subtracted. The rms noise is $0.9 \text{ mJy beam}^{-1} \text{ channel}^{-1}$. Gaussian models have been fit to the spectra, with parameters as given in Table 1. Note that the low-frequency part of the spectrum of Ly α -2 was not sampled by these observations. The [C II] line has a rest frequency of 1900.539 GHz.

(Figure 2) shows emission extending south of the quasar in this velocity range. The deconvolved size of the emission in this velocity range is $\sim 1''.5$ oriented north–south, as derived from Gaussian fitting. This feature could be the result of the tidal interaction or an outflow. We briefly consider the latter possibility.

In order to determine the outflow rate and energetics, we follow the same approach presented in Maiolino et al. (2012), where they detect a similar outflow traced by [C II] in a $z = 6.4$ quasar. More specifically, the luminosity of the high-velocity gas traced by the [C II] provides a lower limit on the mass of outflowing atomic gas (in the extreme limit $n \gg n_c$, the critical density for [C II] excitation). Since the broad component of

[C II] is poorly constrained, we conservatively consider only the luminosity of the [C II] wing integrated between $+220 \text{ km s}^{-1}$ and $+500 \text{ km s}^{-1}$ ($L_{[\text{C II}]}(\text{wing}) = 0.3 \times 10^9 L_\odot$), which gives a lower limit on the outflowing atomic gas mass of $M_{\text{outfl}}(\text{atomic}) > 2.9 \times 10^8 M_\odot$, assuming an abundance ratio of $[\text{C II}]/\text{H} = 1.4 \times 10^{-4}$ (Savage & Sembach 1996). Assuming a simplified conical or bi-conical outflow geometry and a size of $1''.5$ ($=10 \text{ kpc}$), we infer a lower limit on the outflow rate of $\dot{M}_{\text{outfl}} > 80 M_\odot \text{ yr}^{-1}$. This is a modest outflow rate relative to other quasar-driven outflows, which generally have outflow rates higher than a few hundred up to a few thousands $M_\odot \text{ yr}^{-1}$ (Feruglio et al. 2010; Sturm et al. 2011; Cano-Diaz et al. 2012; Maiolino et al. 2012). However, one should keep in mind that

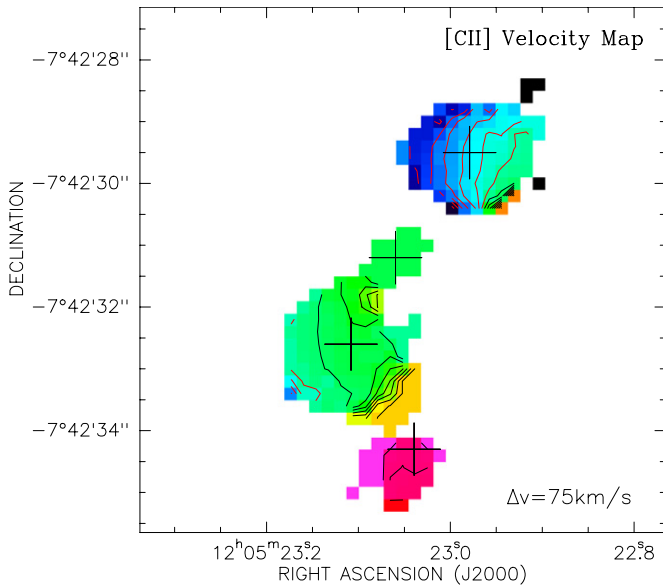


Figure 4. Isovelocity images (1st moment = intensity weighted mean velocity) of the [C II] emission from BRI1202–0725, blanked at 3.5σ . The color scale ranges from -500 km s^{-1} (blue) to $+500 \text{ km s}^{-1}$ (red), and the contours are in steps of 75 km s^{-1} . Crosses are the same as in Figure 2.

this is a lower limit on the total outflow rate, because of the assumed extreme physical conditions, and because a significant fraction of the outflow may be in the molecular phase. We note that by taking the flux of the full broad component used to fit the broad wing (Figure 3(a)), the inferred outflow rate would

increase by a factor of about three. Moreover, this calculation depends critically on the assumed conical geometry and constant velocity, and hence should be considered roughly order of magnitude (see Maiolino et al. 2012 for details).

We derive a lower limit on the kinetic power of $P_K(\text{outfl}) > 5.3 \times 10^{42} \text{ erg s}^{-1}$, which is only 0.2% of the quasar bolometric luminosity ($2.6 \times 10^{45} \text{ erg s}^{-1}$), well below the maximum kinetic power that can be driven by the quasar according to models ($\sim 5\%$; Lapi et al. 2006), meaning that the quasar radiation pressure can easily drive such a mild outflow. On the other hand, this relatively low kinetic power can also be driven by the starburst hosted in the quasar itself. The total IR luminosity of the quasar is $3.3 \times 10^{13} L_\odot$ (Wagg et al. 2012), which implies a star formation rate of $\sim 3300 M_\odot \text{ yr}^{-1}$, for a Charbrier IMF using standard relations (Carilli & Walter 2013). The expected kinetic power is $P_K(\text{SB}) \sim 2 \times 45 \text{ erg s}^{-1}$ (Veilleux et al. 2005). Therefore, in this case, the energetics cannot constrain the nature of the outflow: both the quasar and the starburst can drive it. And again, the derived kinetic luminosity is strictly a lower limit.

4.3. The Ly α Emitters

We have detected [C II] line emission from two narrow-band-selected, Ly α emitting galaxies in the BRI 1202–0725 group at $z = 4.7$. The optical and near-IR properties of Ly α -1 and 2 are described in Hu et al. (1996). The *I*-band magnitudes are 24.2 and 24.5, respectively. Hu et al. (1996) conclude that these galaxies have magnitudes and colors “roughly comparable to an L_* galaxy (at high redshift)” (see also Hu et al. 1997; Lu et al. 1996; Fontana et al. 1996). They also conclude that the Ly α equivalent widths are: “consistent with excitation by the underlying

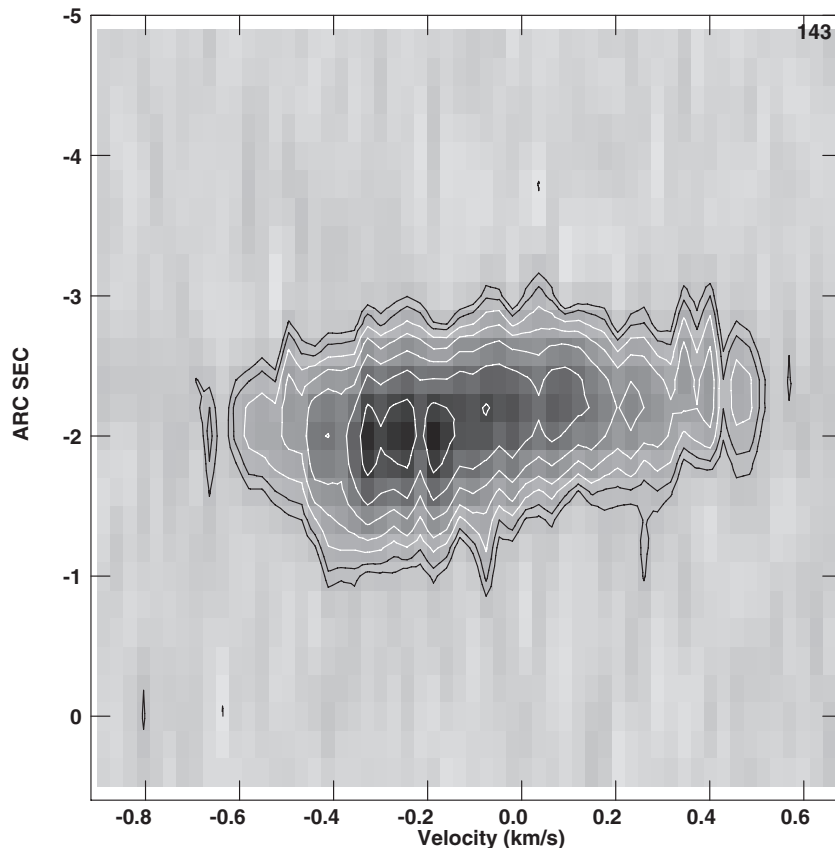


Figure 5. Position–velocity distribution for the SMG in the BRI1202–0725 system, along the east–west direction. Contour levels are a geometric progression in square root two, starting at 2 mJy beam^{-1} . Negative contours are dashed. Zero velocity corresponds to $z = 4.6941$.

[stellar] population,” although they note that the proximity of the quasar raises some interesting questions about ionization (see below). We first consider the submillimeter line and continuum properties of these in the context of star formation.

For Ly α -2, the FIR luminosity is $1.7 \times 10^{12} L_{\odot}$, based on the 340 GHz flux density, and the implied star formation rate derived from the FIR luminosity is $170 M_{\odot} \text{ year}^{-1}$, assuming a standard dust SED and conversion factors (Carilli & Walter 2013). The [C II] line luminosity is $8.2 \times 10^8 L_{\odot}$, based on the symmetrized Gaussian fit shown in Figure 2 (again, this is highly uncertain due to the truncated line profile). Sargsyan et al. (2012) present an empirical relationship between [C II] luminosity and star formation: $\log(\text{SFR}) = \log(L(\text{C II})) - 7.08$ (solar units), derived from observations of the PAH, FIR, and [C II] emission from a large sample of nearby galaxies. For Ly α -2, this relationship would imply a star formation rate of $70 M_{\odot} \text{ year}^{-1}$.

The [C II]/FIR ratio is 0.0005 for Ly α -2. This ratio is comparable to nuclear starburst galaxies seen nearby, and well below the Milky Way ratio of 0.003. However, we emphasize that the [C II] luminosity is uncertain due to the truncated line profile seen in Figure 3, and hence these estimates should be considered at best order of magnitude.

For Ly α -1, the [C II] line luminosity is $1.9 \times 10^8 L_{\odot}$, based on the Gaussian fit shown in Figure 2, with an implied star formation rate of $19 M_{\odot} \text{ year}^{-1}$, using the Sargsyan et al. (2012) relationship. In this case, we only have a lower limit to the FIR luminosity of $3.6 \times 10^{11} L_{\odot}$, based on an upper limit to the 340 GHz flux density of 0.3 mJy, or an upper limit to the star formation rate of $36 M_{\odot} \text{ year}^{-1}$. In this source, the lower limit to the [C II]/FIR ratio is 0.0005.

The proximity of a very luminous quasar to these Ly α emitting galaxies ($L_{1450} \sim 10^{13} L_{\odot}$) presents the possibility that atomic gas is both heated and ionized by the luminous nearby quasar. We ran a series of simple CLOUDY models (Ferland et al. 1998) that reproduced both its Ly α and [C II] luminosities in Ly α -1. We adopted simple models in which a small segment of a spherical shell of gas is located a radial distance 15 kpc from the quasar. We explored an initial density range between 100 and 1000 cm^{-3} , but then pressure equilibrium was assumed between adjacent cells with an initial temperature of 10,000 K. Thus, density climbed to higher values in colder, neutral regions beyond the ionization front. Densities much lower than this required unreasonably high spatial extent of the gas. Densities much higher resulted in very small cloud radial dimensions compared to larger lateral dimensions required by the [C II] 158 μm emission maps.

The gas exhibits the classic “H II” region zone facing the quasar that extends into an ionization front further away, followed by a zone of neutral gas even further away from the quasar. In every case, the Ly α emission arose in the warm $T \sim 10^4$ K, ionized gas, while the 158 μm emission arose in the neutral gas. But at the same time, other standard UV emission lines such as Si IV 1397, N V 1239, and O I 1403 were predicted at luminosities more than a factor of 10 higher than the upper limits placed by Ohya et al. (2004). While these authors did not observe C IV λ 1548, which is the strongest of these transitions, neither has it been detected by other less sensitive observations, which are clearly in conflict with its predicted luminosity of $\sim 10^{42} \text{ erg s}^{-1}$ (Hu et al. 1997). Lowering the metal abundance does not help since many of these transitions serve as important coolants and the gas adjusts to higher temperatures to balance the heat input.

We conclude that the quasar is an unlikely source of heat and ionization for Galaxy Ly α -1. As a result, we speculate that a torus that is optically thick to ionizing photons shields the quasar in the direction of Ly α galaxies (Goosmann & Gaskell 2007). We note that if the FUV heating the PDR arises from the quasar, then the high value of the FUV intensity is likely to produce [O I] 63 μm emission at fluxes comparable to or exceeding the [C II] 158 μm emission. The point here is that at 15 kpc distance, the quasar will produce a $G_0 \sim 1000$, where G_0 is the FUV energy density in units of the Habing ISM value ($G_0 = J_{\nu}/(10^{-19} \text{ erg cm}^{-2} \text{ s}^{-1} \text{ str}^{-1} \text{ Hz}^{-1})$). As Kauffmann et al. (1999) have shown, PDRs with $G_0 > 1000$ result in an intensity ratio [O I] 63 μm /[C II] 158 μm > 1 , owing to the relatively high temperature of the gas. Thus, the detection of the 63 μm transition at fluxes comparable to or greater than that of the 158 μm line indicates a relatively high value of G_0 . This would be consistent with incidence FUV flux coming from the quasar, or local heating by a luminous O star located within a few pc from the gas. An intensity ratio $\ll 1$ would certainly rule out the gas irradiated by such an intense radiation field.

5. DISCUSSION

BRI 1202–0725 shows all the attributes expected during massive galaxy and SMBH formation in a dense group in the early universe. The system has four interacting galaxies within 5'' of each other (35 kpc in projection): two hyper-starbursts (an SMG and a quasar host), and two Ly α -emitting galaxies (Ly α -1 and 2). Impressively, all are detected in [C II] emission.

Perhaps the most impressive result from these observations is the relative ease with which high-redshift Ly α -selected galaxies can be detected in [C II] emission. Using only 1/3 of the full ALMA, both Ly α -1 and 2 were detected at reasonable signal to noise in just 20 minutes. Scaling to the full ALMA, and a still reasonable 3 hr integration, leads a factor of 10 increase in sensitivity, allowing for detailed imaging of the atomic gas on sub-kpc scales in normal star-forming galaxies (star formation rates \sim few to $10 M_{\odot} \text{ year}^{-1}$) at very high redshift. [C II] observations with ALMA open a new window on dynamical studies of the first galaxies.

An interesting trend for the [C II] emission in the vicinity of the quasar is for the atomic gas to extend in the direction of Ly α -1 and 2. In fact, Ly α -1 may be a local maximum within a possible bridge of atomic gas connecting the quasar and the SMG, as expected during major mergers of gas-rich galaxies (Barnes & Hernquist 1996; Li et al. 2007). Unfortunately, the current resolution is insufficient to distinguish between a true bridge, or simply a blurring of independent [C II] emission from the quasar and G3. An argument for some physical connection is the velocity continuity from the quasar through G3. A critical observation will be to confirm this bridge with deeper, higher resolution observations with ALMA, as well as to confirm the [C II] line and detect dust continuum emission from Ly α -1.

The presence of a luminous quasar would naturally lead to strong outflows, as has been seen in both low- and high-redshift quasars in CO and/or [C II] emission (Maiolino et al. 2012; Sturm et al. 2011). Outflow from the quasar in BRI 1202–0725 is suggested by the presence of an associated broad absorption line system (Capellupo et al. 2011), although this could also be of tidal origin. Our analysis of the broad [C II] wing of the quasar indicates that while an outflow may be present, it is not likely to dominate the gas depletion in the quasar host galaxy. Indeed, at the current outflow rate, the available gas mass ($\sim 5 \times 10^{10} M_{\odot}$)

would be expelled in about 6×10^8 yr, which is much longer than the star formation consumption timescale ($\sim 10^7$ yr).

The [C II] emission from the SMG shows a clear, relatively smooth velocity gradient over a scale of $\sim 1''$ in an east–west PV plot, and in the first moment image, and a smooth-integrated emission line profile over a broad range in velocity (700 km s^{-1}). The morphology seen in the east–west PV plot, and the spectral profile, for the [C II] emission differ from the CO 5–4 emission, which appears more “clumpy” (two distinct peaks) in both the PV plot and in the spectrum (Sargsyan et al. 2012). High-order CO emission traces higher density gas, $> 10^3 \text{ cm}^{-3}$, while [C II] traces both the high-density gas in PDRs, and lower density atomic gas (CNM). Hence, it could be that the lower density atomic gas has a smoother overall distribution than the CO, filling-in the velocity and spatial gaps seen in CO. Higher resolution CO and [C II] observations are required to delineate the relative atomic and molecular gas distributions in BRI 1202–0725.

Simpson et al. (2012) recently presented evidence that FIR luminous quasars are a short (1 Myr) but ubiquitous phase during the evolution of a dust obscured gas-rich starburst to an unobscured, gas poor quasar. The narrower CO line width in the quasar relative to the SMG in BRI1202–0725, and the apparently more spatially extended gas distribution (as seen from the dynamics) in the SMG, are consistent with the trends discussed by Simpson et al. However, in BRI1202–0725, we see the quasar and SMG phases as coeval, with both galaxies involved in the gas-rich merger. It is unclear how such a hyper-starburst galaxy pair, one of which is a luminous broad line quasar, fit into the stated evolutionary model.

C.L.C. thanks the Kavli Institute for Cosmology for their hospitality. We thank the referee for useful comments. This paper makes use of the following ALMA data: ADS/JAO.ALMA#2011.0.00006.SV. ALMA is a partnership of ESO (representing its member states), NSF (USA), and NINS (Japan), together with NRC (Canada) and NSC and ASIAA (Taiwan), in cooperation with the Republic of Chile. The Joint ALMA Observatory is operated by ESO, AUI/NRAO, and NAOJ.

REFERENCES

- Andreon, S., & Huertas-Company, M. 2011, *A&A*, 526, 11
 Barnes, J., & Hernquist, L. 1996, *ApJ*, 471, 115
 Blain, A., Smail, I., Ivison, R., Kneib, J. P., & Frayer, D. 2002, *PhR*, 369, 111
 Bennett, C. L., Fixsen, D., Hinshaw, G., et al. 1994, *ApJ*, 434, 587
 Cano-Diaz, M., Maiolino, R., Marconi, A., et al. 2012, *A&A*, 537, L8
 Capellupo, D. M., Hamann, F., Shields, J. C., et al. 2011, *MNRAS*, 413, 908
 Carilli, C. L., Kohno, K., Kawabe, R., et al. 2002, *AJ*, 123, 1838
 Carilli, C. L., & Walter, F. 2013, *ARA&A*, in press
 Cornwell, T., Braun, R., & Briggs, D. 1999, in ASP Conf. Ser. 180, Synthesis Imaging in Radio Astronomy II, ed. G. B. Taylor, C. L. Carilli, & R. A. Perley (San Francisco, CA: ASP), 151
 Crawford, M. K., Lugten, J., Fitelson, W., Genzel, R., & Melnick, G. 1986, *ApJL*, 303, 57
 Ferland, G. J., Korista, K. T., Verner, D. A., et al. 1998, *PASP*, 110, 761
 Feruglio, C., Maiolino, R., Piconcelli, E., et al. 2010, *A&A*, 518, L155
 Fontana, A., Cristiani, S., D’Odorico, S., Giallongo, E., & Savaglio, S. 1996, *MNRAS*, 279, L27
 Genzel, R., & Cesarsky, C. 2000, *ARA&A*, 38, 761
 Goosmann, R., & Gaskell, C. 2007, *A&A*, 465, 129
 Haaring, N., & Rix, H. 2004, *ApJL*, 604, 89
 Hu, E. M., McMahon, R. G., & Egami, E. 1996, *ApJL*, 459, 53
 Hu, E. M., McMahon, R. G., & Egami, E. 1997, in Proc. 37th Herstmonceux Conf., ed. N. R. Tanvir, A. Aragon-Salamanca, & J. V. Wall (Singapore: World Scientific), 91
 Iono, D., Yun, M. S., Elvis, M., et al. 2006, *ApJL*, 645, 97
 Isaak, K., McMahon, R. G., Hills, R. E., & Withington, S. 1994, *MNRAS*, 269, L28
 Kauffmann, G., Colberg, J. M., Diaferio, A., & White, S. D. M. 1999, *MNRAS*, 307, 529
 Khandai, N., Feng, Y., DeGraf, C., et al. 2012, *MNRAS*, 423, 2397
 Klamer, I., Ekers, R., Sadler, E., et al. 2004, *ApJL*, 612, 97
 Kurk, J. 2009, *A&A*, 504, 331
 Lapi, A., Shankar, F., Mao, J., et al. 2006, *ApJL*, 650, 42
 Levshakov, S., Reimers, D., Kozlov, M. G., Porsev, S. G., & Molaro, P. 2008, *A&A*, 479, 719
 Li, Y., Herquist, L., Robertson, B., et al. 2007, *ApJ*, 665, 187
 Lu, L., Sargent, W. L. W., Womble, D. S., & Barlow, T. A. 1996, *ApJ*, 457, 1
 Maiolino, R., Gallerani, S., Neri, R., et al. 2012, *MNRAS*, 425, L66
 Malhotra, S., Helou, G., Stacey, G., et al. 1997, *ApJL*, 491, 27
 Momjian, E., Carilli, C. L., & Petric, A. O. 2005, *AJ*, 129, 1809
 Ohta, K., Matsumoto, T., Maihara, T., et al. 2000, *PASJ*, 52, 557
 Ohta, K., Yamada, T., Nakanishi, K., et al. 1996, *Natur*, 382, 426
 Ohya, Y., Taniguchi, Y., & Shioya, Y. 2004, *AJ*, 128, 2704
 Omont, A., Petitjean, P., Guilleaume, S., et al. 1996, *Natur*, 382, 428
 Papadopoulos, P., Isaak, K., & van der Werf, P. 2010, *ApJ*, 711, 757
 Petitjean, P., Pecontal, E., Valls-Gabaud, D., & Charlot, S. 1996, *Natur*, 380, 411
 Salome, P., Guélin, M., Downes, D., et al. 2012, *A&A*, 545, 57
 Sargsyan, L., Lebouteiller, V., Weedman, D., et al. 2012, *ApJ*, 755, 171
 Simpson, J. M., Smail, I., Swinbank, A. M., et al. 2012, *MNRAS*, 426, 3201
 Savage, B., & Sembach, K. 1996, *ARA&A*, 43, 677
 Solomon, P., & Downes, D. 1998, *ApJ*, 507, 615
 Stacey, G., Hailey-Dunsheath, S., Ferkinhoff, C., et al. 2010, *ApJ*, 725, 957
 Sturm, E., González-Alfonso, E., Veilleux, S., et al. 2011, *ApJL*, 733, 16
 Veilleux, S., Cecil, G., & Bland-Hawthorn, J. 2005, *ARA&A*, 43, 769
 Wagg, J., Wiklind, T., Carilli, C. L., et al. 2012, *ApJL*, 752, 30
 Wang, R., Carilli, C., Neri, R., et al. 2010a, *ApJ*, 714, 699
 Wang, R., Wagg, J., Carilli, C., et al. 2011, *AJ*, 142, 101
 Wang, R., Wagg, J., Carilli, C., et al. 2010b, *ApJL*, 739, 34
 Wright, E., Mather, J., Bennett, C., et al. 1991, *ApJ*, 381, 200
 Yun, M. S., & Carilli, C. 2002, *ApJ*, 568, 88
 Yun, M. S., Carilli, C. L., Kawabe, R., et al. 2000, *ApJ*, 528, 171